Solution-processed Cesium Hexabromopalladate(IV), Cs_2PdBr_6, for Optoelectronic Applications

Nobuya Sakai[†], Amir Abbas Haghighirad[†], Marina R. Filip[§], Pabitra K. Nayak[†], Simantini Nayak[#], Alexandra Ramadan[†], Zhiping Wang[†], Feliciano Giustino[§] and Henry J. Snaith[†*]

[†]Department of Physics, University of Oxford, Clarendon Laboratory, Parks Road, Oxford, OX1 3PU, United Kingdom

[§]Department of Materials, University of Oxford, 16 Parks Road, Oxford OX1 3PH, United Kingdom

[#]Department of Chemistry, University of Oxford, Inorganic Chemistry Laboratory, South Parks Road, Oxford, OX1 3QR, United Kingdom

Supporting Information Placeholder

ABSTRACT: Lead halide perovskites are materials with excellent optoelectronic and photovoltaic properties. However, some hurdles remain prior to commercialization of these materials, such as chemical stability, phase stability, sensitivity to moisture, and potential issues due to the toxicity of lead. Here, we report a new type of lead-free perovskite related compound, Cs_2PdBr_6. This compound is solution processable, exhibits long-lived photoluminescence, and an optical band gap of 1.6 eV. Density functional theory calculations indicate that this compound has dispersive electronic bands, with electron and hole effective masses of 0.53 and 0.85 m_e, respectively. In addition, Cs_2PdBr_6 is resistant to water, in contrast to lead-halide perovskites, indicating excellent prospects for long-term stability. These combined properties demonstrate that Cs_2PdBr_6 is a promising novel compound for optoelectronic applications.

Recent research on the properties of lead-halide perovskites have attracted significant attention due to their excellent optoelectronic and photovoltaic properties, and the ability to manufacture high quality polycrystalline thin films by low-cost solution processing.[1–4] Metal halide perovskites have the general formula ABX_3, where A= CH_3NH_3, $HC(NH_2)_2$ and Cs; B = Pb and/or Sn; X= I, Br and Cl.[5–13] The presence of lead and the long-term stability (i.e. chemical and structural) are the main issues, that need addressing, and will have a great impact on future technologies.[14,15] Although the presence of lead in the highest quality perovskite semiconductors is most likely tolerable for photovoltaic solar energy applica

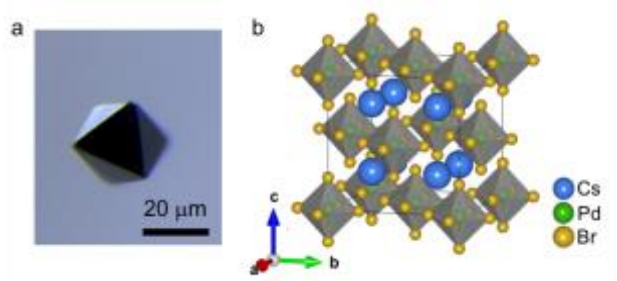

Figure 1. (a) Optical microscope image of a Cs_2PdBr_6 single crystal. (b) 3D crystal structure of Cs_2PdBr_6 showing the unit cell.

tions,[16] for other applications as semiconductors for electronics and optoelectronics this may constitute a barrier, since those devices are unlikely to be exempt from compliance to the restriction of hazardous substances (RoHS). The recently discovered new family of double perovskites with the formula $A_2B'B''X_6$, (B′ = Sb^{3+}, Bi^{3+} and B″ = Cu^+, Ag^+, Au^+) provide promising environmentally-friendly and stable series of materials for optoelectronic applications.[17–20] In addition, it is also possible to replace the B-site cation in $A_2B'B''X_6$ with a vacancy, resulting in a vacancy-ordered defect-variant perovskite with the chemical formula A_2BX_6. Recently, A_2BX_6 compounds with B = Sn and Te have been reported to absorb light in the visible to infrared (IR) region and provide new opportunities for less-toxic and chemically stable optoelectronic materials.[21–23] Here, we report a new A_2BX_6 compound with A= Cs^+, B= Pd^{4+} and X= Br^- synthesized from a solution process.

To prepare Cs_2PdBr_6 single crystals, we dissolved 2M CsBr and 1M PdBr2 in 5 mL aqueous HBr (48 wt. % in H_2O) solution and placed the solution in a box furnace at 85 °C for 5 min. We then added 10 vol% of dimethyl sulfoxide (DMSO) into the hot precursor solution kept at 120 °C on the hot plate. Immediately, black Cs_2PdBr_6 crystals precipitated from the solution and were collected (we give a detailed description for all experiments in the SI).

We show the optical microscope (OM) image of a black lustrous octahedral shaped crystal of Cs_2PdBr_6 (lateral size of 30 μm) in Figure 1a. We observe sharp Bragg peaks (see Figure S1) with the selection rules characteristic of $Fm\bar{3}m$ symmetry revealing absences [hkl; $h + k$, $k + l$, ($h + l = 2n$)] corresponding to face-centered space groups $F432$, $F\bar{4}3m$ and $Fm\bar{3}m$. We find that the crystallographic data is consistent with the space group $Fm\bar{3}m$ (no. 225).[24] We summarize all the details of crystallographic refinements in Table S1. Using the crystallographic data, we have simulated the unit cell, which we show in Figure 1b. We confirm the phase purity and the crystal structure of the polycrystalline sample of Cs_2PdBr_6 (i.e. powder and thin-film) by powder X-ray diffraction (PXRD) (shown in Figure S2). The measured PXRD patterns are in a good agreement with the calculated single crystal data.

Here, we propose the formation mechanism of Cs_2PdBr_6. In our starting solution, we use $PdBr_2$ where Pd is in its 2+ oxidation sate. However, from the XRD measurements and crystallographic refinement, the structure is only consistent with Pd in the 4+ oxidation state. As we do not add any external oxidizing agent to the solution, the oxidizing agent must have been generated *in-situ*. We monitor the changes in the salt solution using attenuated total reflection infrared (ATR-IR) spectroscopy. In Figure S3, we show the IR spectrum of $PdBr_2$ solution in DMSO and after the addition of HBr to the solution. We see that the absorbance peak around 1045 cm^{-1} that corresponds to absorbance of S=O[25] bond shifts to 1008 cm^{-1} after the addition of HBr. This shift of absorbance peak to a lower energy indicates that the bond order of S-O bond in DMSO changes due to the formation of DMSO-HBr adduct. HBr: DMSO is known to function as the oxidizing agent in organic synthesis, as well as oxidization of metals.[26,27] Here, HBr: DMSO oxidizes Pd^{2+} to Pd^{4+} and the available bromide ions in HBr: DMSO leads to the formation of $[PdBr_6]^{-2}$, which is then the building block to form the compound with Cs^+ as the counter ion. The oxidation of Pd (II) and formation of a new complex are often associated with a change in the absorbance spectrum. We monitor the change in the UV-Vis absorption spectrum of $PdBr_2$ in DMSO as a function of added HBr (see Figure S4). We observe the absorbance around 415 nm increases with the addition of HBr. For a control system without the $PdBr_2$ salt, we do not see such a change in the UV-Vis spectrum. To find out if HBr: DMSO system is essential for the formation of Cs_2PdBr_6, we perform a single crystal study with a single-crystal fabricated from CsBr: $PdBr_2$ (2:1) in HBr (i.e. without DMSO). In Figure S5 we show the optical microscopy image of single-crystals from the above-mentioned solution which are reddish neddle-like crystals, in contrast to the Cs_2PdBr_6, which forms as octahedral shaped crystals. The single crystal XRD analysis shows sharp Bragg peaks in $2/m$ Laue class and further analysis confirms the space group $P2_1/c$ and the chemical composition of $Cs_2PdBr_4{\cdot}xH_2O$. In the latter composition, Pd^{2+} is in a square planar coordination (see Table S2 and Figure S6). These results help us understand the role of HBr: DMSO in formation of Cs_2PdBr_6. More information about the intermediates and end products during the formation of Cs_2PdBr_6, in the HBr: DMSO system requires further investigations beyond the scope of this work.

In order to investigate the optoelectronic properties of Cs_2PdBr_6, we calculate the electronic band

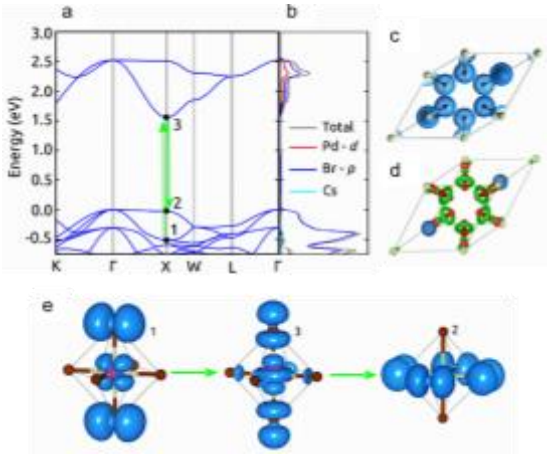

Figure 2. (a) Electronic band structure of Cs_2PdBr_6 on the high symmetry path: K ($3\pi/2a$, $3\pi/2a$, 0) –Γ (0,0,0) - X (0, $2\pi/a$, 0) - W (π/a, $2\pi/a$, 0)- L (π/a, π/a, π/a) -Γ, where ($a/2$, 0, $a/2$), ($a/2$, $a/2$, 0) and (0, $a/2$, $a/2$) are the lattice vectors of the FCC lattice. The black dots mark the second highest (1) and highest (2) occupied state and the lowest unoccupied state (3) at the X-point. The green arrows mark the 1-3 and 2-3 optical transitions discussed in the text. (b) Projected density of states. (c) 3D plot of the total charge density and (d) the bonding charge density. The red regions correspond to the

negative bonding charge density and the green regions correspond to the positive bonding charge density. (e) 3D plot of the wave-function distribution at the points marked (1), (2) and (3) on the band structure in (a).

structure within the generalized gradient approximation to density functional theory (DFT/GGA)[28,29] and correct the underestimated band gap using the Heyd-Scuseria-Ernzerhof (HSE) hybrid functional.[30,31] As shown in Table S3 and Figures 2a and b, we obtain an indirect fundamental bandgap between Γ (valence band top) and X (conduction band bottom) of 1.56 eV from DFT-HSE. However, from Figure 2a we also note that the lowest direct band gap (at the X-point) is only marginally larger than the indirect band gap (1.59 eV). Given that the difference between the calculated direct and indirect band gaps is of only 30 meV, more advanced electronic structure calculations would be required to unambiguously assign the nature of the gap. In addition, we also calculate the isotropic electron and hole effective masses at the X and Γ points, respectively, within DFT/PBE (Table S3), as described in Ref[32] and the SI. The electrons have a smaller effective mass to the light holes (0.53 vs 0.85 m_e, respectively), while the heavy hole effective masses are two orders of magnitude larger (19.9 m_e). Owing to the presence of the heavy hole band at the top of the valence band, and the low electron effective masses, we expect that Cs_2PdBr_6 will behave as an *n*-type semiconductor, with a higher electron mobility to hole mobility. In Figure 2c and d, we show the total charge density distribution calculated within DFT/GGA and the charge density of the non-interacting atoms placed at the crystallographic sites (bonding charge density). Figure 2c shows that the electrons are either localized in the $PdBr_6$ octahedra or on the Cs cation, in a close resemblance to $CH_3NH_3PbI_3$.[32,33] In Figure 2d, we confirm the non-bonding character of the electrons localized on Cs. Additionally, this calculation displays a redistribution of the electrons primarily around the Br^- ions (green rings) directed towards the interstitial space between the isolated octahedra. This redistribution of charge can explain why the band structure displays such a dispersive profile, despite the absence of the corner-sharing connectivity of the $PbBr_6$ octahedra. In Figure S7, we show a calculated independent-particle optical absorption spectrum, without taking into account phonon-assisted processes or electron-hole interaction (see SI for calculation details). We observe a sharp increase in the calculated absorption coefficient at 600 nm (2.07 eV) which corresponds to the transitions 1-3 on the band structure in Figure 2 (a). We observe the absorption onset at approximately 780 nm (1.59 eV), which is similar to the direct band gap at the X-point (i.e. the transition 2-3). The difference in the oscillator strengths at these two photon energies can be

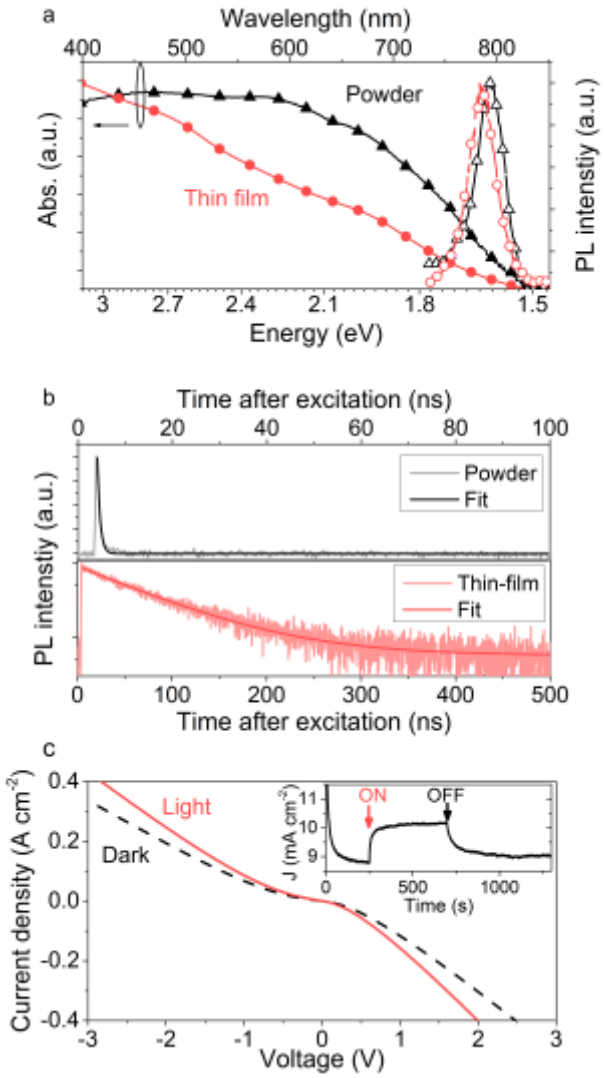

Figure 3. (a) UV-vis absorption, steady-state PL and (b) Time-resolved PL decay of a Cs_2PdBr_6. (c) J-V curves on a ITO/Cs_2PdBr_6/Ag junction device under the dark and simulated sun light (100 mW cm^{-2}, AM 1.5). Insert: photo-generated current density under simulated solar light over time at a fixed voltage at -0.5V.

rationalized qualitatively from the distribution of the electronic wave functions at states 1, 2 and 3 (shown in Figure 2). As we observe in Figure 2 (e), the 1-3 optical transition occurs between electronic states localized at the same crystal site, in contrast to the 2-3 transition, which explains the large difference in the strength of the dipole matrix elements. We note that the optical transitions are dipole-forbidden right

at the X-point, but become allowed as soon as the wave vector is slightly off X. We present a more detailed analysis of all electronic structure calculations in the SI.

To investigate experimentally the optoelectronic properties of Cs_2PdBr_6, we performed UV-visible absorption and steady-state photoluminescence (PL) measurements on the single crystals and thin film, which we show in Figure 3a. The absorption onset on the single crystal appears at ~784 nm (1.58 eV), and the PL spectra show PL emission maximum at 772 nm (1.60 eV), respectively. We deduce the absorption onset at 1.58 eV by Kubelka-Munk function (F(R)) theory as shown in Figure S8, which we show a correlation between photon energy and F(R)[34–36] to take into account for the contribution of the scattering from the single crystal sample. The optical spectrum of a thin-film spin-coated from a solution of dissolved single crystals in DMF also shows the optical band gap of ~ 1.60 eV, in good agreement with the DFT-HSE calculations. From our combined experimental and theoretical analysis of the optoelectronic properties of Cs_2PdBr_6 we propose that light absorption mainly takes place through the higher energy transitions (1-3 in Figure 2a and S7) while the electron-hole recombination should be associated with 2-3 transitions at the band edges (shown in Figures 2a and S7). In Figure 3b, we show a time resolved photoluminescence (TRPL) decay of a single crystal and a thin film. We fitted the early decay by a mono-exponential function with decay times of 1.85 ns and 79 ns, respectively. This long lifetime and direct band-to-band transition from Cs_2PdBr_6 are very encouraging indicators for their potential applications in optoelectronic devices.

A similar material Cs_2SnI_6, has attracted attention for their potential applications in air-stable optoelectronic devices,[21–23,37–40], however, the material can have defects due to the halide and tin vacancies.[40] To find out whether Cs_2PdBr_6 has significant amount of density of states in the bandgap, we have used the surface photo voltage (SPV) study using sub band gap illumination at 850 nm (i.e. 1.46 eV). Presence of electronic states in the bandgap region gives SPV response, however, as we show in the Figure S9, we do not see any response from sub bandgap illumination confirming that the presence of electronic states in the bandgap region in these material is not very significant. We do note however, that there may be defects states present in the material which could result in non-radiative recombinations, which would need to be passivated. As this material is in the early stage of development, a further study of defect states would help to improve the electronic quality of the material.[41] We use ultraviolet photoemission spectroscopy (UPS) to determine the energetic band levels in Cs_2PdBr_6 thin films and we show the UPS spectrum in Figure S10. We determine that the valence band position is determined from the secondary electron cut-off (SECO) region. The valence band maximum (VBM) of a Cs_2PdBr_6 thin film is located at -6.47 eV with respect to the vacuum level, whereas the Fermi level of the material is at -4.95 eV, close to the conduction band minimum of -4.86 eV (calculated by subtracting the optical band gap from the VBM). The Fermi-level position is consistent with an *n*-type nature of this material, and potentially a shallow donor level existing. The conduction and valance band energy levels are relatively deep, as compared to the archetypical $CH_3NH_3PbI_3$ perovskite, which may make this material more challenging to integrate into devices, where it needs to be coupled with electron and hole charge extraction layers.

In order to assess whether Cs_2PdBr_6 is photoconductive, we fabricate a simple "sandwich-structure" device of ITO/Cs_2PdBr_6/Ag junction and characterize this by current density–voltage (*J-V*) measurement under ambient conditions, as we show in Figure 3c. We find that the Cs_2PdBr_6 thin-film on an ITO substrate displays a uniform surface, which we show in Figure S11. In Figure 3c, we show the *J-V* characteristics in dark and under AM1.5 simulated solar light at 100 $mWcm^{-2}$. As an inset of Figure 3c, we show the transient photo-response of the conductivity of the device, measured at -0.5 V applied bias. Although the simple diode we present does not exhibit significant rectification, we do observe an increase in conductivity under illumination. This is consistent with the fact that Cs_2PdBr_6 is a semiconductor that shows a photo-responsive behavior. In addition, we measured the 4-point probe conductivity of Cs_2PbBr_6 thin films processed on glass, and determined a dark conductivity of 2.5×10^{-5} Scm^{-1}. This is in a similar range to the dark conductivity of the doped organic charge collection layers.[42]

Finally, to examine the chemical and phase stability of Cs_2PdBr_6, we carry out a water tolerance test on the Cs_2PdBr_6 crystals. We put Cs_2PdBr_6 crystals in water at room temperature for 10 min. Figure S12 shows the comparison of PXRD patterns and optical microscopy images before and after the water immersion test. We do not see any obvious difference reminiscent of phase change and chemical decomposition of crystallites after these were

immersed in H_2O. This clearly shows that Cs_2PdBr_6 is a water stable compound.

In summary, we have made a new semiconductor material, Cs_2PdBr_6, which is synthesized from a solution process, enabled by an *in-situ* oxidization of Pd^{2+} to Pd^{4+} during synthesis. This method has not been considered for the synthesis of palladium-based materials, nor other A_2MX_6 compounds. Cs_2PdBr_6 crystallizes in a cubic crystal structure with space group $Fm\bar{3}m$. Cs_2PdBr_6 shows remarkable structure and chemical stability, unlike Pb-based halide perovskites. Electronic structure calculations within DFT-HSE, as well as optical absorption and PL measurements confirm that this compound has a band gap of 1.6 eV. In addition, the photo-response in an ITO/Cs_2PdBr_6/Ag device indicates that Cs_2PdBr_6 can be employed into a wide range optoelectronic applications such as photon-sensors, light-emitting diodes and PV devices.

ASSOCIATED CONTENT

The Supporting Information is available free of charge on the ACS Publications website at DOI: XXXX. Experimental details, crystallographic data, morphological data, spectra data, and DFT calculation details, including Figures S1–S10 and Table S1-S3 (PDF)

AUTHOR INFORMATION

Corresponding Author

[*]Henry.Snaith@physics.ox.ac.uk

Author Contributions

[#]N.S. and A.A.H contributed equally to this work.

ACKNOWLEDGMENT

This research has mainly received funding from the European Commission (FP7/2007– 2013 grant no. 604032), Engineering and Physical Science Research Council (EP/L024667/1 and EP/M015254/1). MRF and FG have received funding from the Graphene Flagship (EU FP7H2020 grant no. 696656604391 Graphene-Core1), the Leverhulme Trust (Grant RL-2012-001), the UK Engineering and Physical Sciences Research Council (Grant No. EP/J009857/1). MRF and FG acknowledge the use of the University of Oxford Advanced Research Computing (ARC) facility (http://dx.doi.org/10.5281/zenodo.22558) and the ARCHER UK National Supercomputing Service under the 'AMSEC' Leadership project. PN and SN are supported by Marie Skłodowska-Curie actions individual fellowships (grant agreement number 653184 and 659306, respectively). Figures involving atomic structures were rendered using VESTA [13].

REFERENCES

(1) Stranks, S. D.; Snaith, H. J. *Nat. Nanotechnol.* **2015**, *10* (5), 391.
(2) Zhang, W.; Eperon, G. E.; Snaith, H. J. *Nat. Energy* **2016**, *1*, 16048.
(3) Sutherland, B. R.; Sargent, E. H. *Nat. Photonics* **2016**, *10* (5), 295.
(4) Manser, J. S.; Christians, J. A.; Kamat, P. V. *Chem. Rev.* **2016**.
(5) Lee, M. M.; Teuscher, J.; Miyasaka, T.; Murakami, T. N.; Snaith, H. J. *Science.* **2012**, *338* (6107), 643.
(6) Chung, I.; Lee, B.; He, J.; Chang, R. P. H.; Kanatzidis, M. G. *Nature* **2012**, *485* (7399), 486.
(7) Hao, F.; Stoumpos, C. C.; Cao, D. H.; Chang, R. P. H.; Kanatzidis, M. G. *Nat. Photonics* **2014**, 8, 489.
(8) Koscher, B. A.; Bronstein, N. D.; Olshansky, J. H.; Bekenstein, Y.; Alivisatos, A. P. *J. Am. Chem. Soc.* **2016**, *138* (37), 12065.
(9) Lee, S. J.; Shin, S. S.; Kim, Y. C.; Kim, D.; Ahn, T. K.; Noh, J. H.; Seo, J.; Seok, S. Il. *J. Am. Chem. Soc.* **2016**, *138* (12), 3974.
(10) Fabini, D. H.; Laurita, G.; Bechtel, J. S.; Stoumpos, C. C.; Evans, H. A.; Kontos, A. G.; Raptis, Y. S.; Falaras, P.; Van der Ven, A.; Kanatzidis, M. G.; Seshadri, R. *J. Am. Chem. Soc.* **2016**, *138* (36), 11829.
(11) Liao, W.; Zhao, D.; Yu, Y.; Shrestha, N.; Ghimire, K.; Grice, C. R.; Wang, C.; Xiao, Y.; Cimaroli, A. J.; Ellingson, R. J.; Podraza, N. J.; Zhu, K.; Xiong, R.-G.; Yan, Y. *J. Am. Chem. Soc.* **2016**, *138* (38), 12360.
(12) Eperon, G. E.; Stranks, S. D.; Menelaou, C.; Johnston, M. B.; Herz, L. M.; Snaith, H. J. *Energy Environ. Sci.* **2014**, *7* (3), 982.
(13) Noel, N. K.; Stranks, S. D.; Abate, A.; Wehrenfennig, C.; Guarnera, S.; Haghighirad, A.-A.; Sadhanala, A.; Eperon, G. E.; Pathak, S. K.; Johnston, M. B.; Petrozza, A.; Herz, L. M.; Snaith, H. J. *Energy Environ. Sci.* **2014**, *7*, 3061.
(14) Wang, D.; Wright, M.; Elumalai, N. K.; Uddin, A. *Sol. Energy Mater. Sol. Cells* **2016**, *147*, 255.
(15) Babayigit, A.; Duy Thanh, D.; Ethirajan, A.; Manca, J.; Muller, M.; Boyen, H.-G.; Conings, B. *Sci. Rep.* **2016**, *6*, 18721.
(16) Green, M. A.; Ho-Baillie, A.; Snaith, H. J. *Nat. Photonics* **2014**, *8* (7), 506.
(17) Slavney, A. H.; Hu, T.; Lindenberg, A. M.; Karunadasa, H. I. *J. Am. Chem. Soc.* **2016**, *138* (7), 2138.
(18) Volonakis, G.; Filip, M. R.; Haghighirad, A. A.; Sakai, N.; Wenger, B.; Snaith, H. J.; Giustino, F. *J. Phys. Chem. Lett.* **2016**, *7* (7), 1254.
(19) Giustino, F.; Snaith, H. J. *ACS Energy Lett.* **2016**, *1* (6), 1233.
(20) McClure, E. T.; Ball, M. R.; Windl, W.; Woodward, P. M. *Chem. Mater.* **2016**, *28* (5), 1348.
(21) Tei, C.; Maughan, A. E.; Ganose, A. M.; Bordelon, M. M.; Miller, E. M.; Scanlon, D. O.; Neilson, J. R. *J. Am. Chem. Soc.* **2016**, *138* (27), 8453.
(22) Lee, B.; Stoumpos, C. C.; Zhou, N.; Hao, F.; Malliakas, C.; Yeh, C.-Y.; Marks, T. J.; Kanatzidis, M. G.; Chang, R. P. H. *J. Am. Chem. Soc.* **2014**, *136* (43), 15379.
(23) Saparov, B.; Sun, J. P.; Meng, W.; Xiao, Z.; Duan, H. S.; Gunawan, O.; Shin, D.; Hill, I. G.; Yan, Y.; Mitzi, D. B. *Chem. Mater.* **2016**, *28* (7), 2315.
(24) Knox, K.; Mitchell, D. W. *J. Inorg. Nucl. Chem.* **1961**, *21* (9), 253.
(25) Fawcett, W. R.; Kloss, A. a. *J. Phys. Chem.* **1996**, *100* (6), 2019.
(26) Karki, M.; Magolan, J. *J. Org. Chem.* **2015**, *80* (7), 3701.
(27) Shirshova, L. V; Kokoreva, S. G.; Lavrent, I. P. **2008**, *57* (12), 2447.
(28) P, Hohenberg. W, K. *Phys. Rev. B* **1964**, *136* (3B), B864.
(29) Perdew, J. P.; Burke, K.; Ernzerhof, M. *Phys. Rev. Lett.* **1996**, *77* (18), 3865.
(30) Heyd, J.; Scuseria, G. E.; Ernzerhof, M. *J. Chem. Phys.* **2003**, *118* (18), 8207.
(31) Heyd, J.; Scuseria, G. E.; Ernzerhof, M. *J. Chem. Phys.* **2006**, *124* (21).
(32) Filip, M. R.; Verdi, C.; Giustino, F. *J. Phys. Chem. C* **2015**, *119* (45), 25209.
(33) Filip, Marina R Eperon, Giles E Snaith, J. H.; Giustino, F. *Nat. Commun.* **2014**, *5*, 1.
(34) Kubelka, P. *J. Opt. Soc. Am.* **1948**, *38* (5), 448.
(35) Nobbs, J. H. *Rev. Prog. Color. Relat. Top.* **1985**, *15* (1), 66.
(36) Džimbeg-malčić, V.; Barbarić-mikočević, Ž.; Itrić, K. *Tech. Gaz.* **2011**, *18* (1), 117.
(37) Qiu, X.; Cao, B.; Yuan, S.; Chen, X.; Qiu, Z.; Jiang, Y.; Ye, Q.; Wang, H.; Zeng, H.; Liu, J.; Kanatzidis, M. G. *Sol. Energy Mater. Sol. Cells* **2017**, *159*, 227.
(38) Qiu, X.; Jiang, Y.; Zhang, H.; Qiu, Z.; Yuan, S.; Wang, P.; Cao, B. *Phys. status solidi - Rapid Res. Lett.* **2016**, *591* (8), 587.

(39) Kaltzoglou, A.; Antoniadou, M.; Kontos, A. G.; Stoumpos, C. C.; Perganti, D.; Siranidi, E.; Raptis, V.; Trohidou, K. N.; Psycharis, V.; Kanatzidis, M. G.; Falaras, P. *J. Phys. Chem. C* **2016**, *120*, (22), 11777.
(40) Xiao, Z.; Zhou, Y.; Hosono, H.; Kamiya, T. *Phys. Chem. Chem. Phys.* **2015**, *17* (29), 18900.
(41) Zhang, W.; Pathak, S.; Sakai, N.; Stergiopoulos, T.; Nayak, P. K.; Noel, N. K.; Haghighirad, A. A.; Burlakov, V. M.; deQuilettes, D. W.; Sadhanala, A.; Li, W.; Wang, L.; Ginger, D. S.; Friend, R. H.; Snaith, H. J. *Nat. Commun.* **2015**, *6*, 10030.
(42) Abate, A.; Hollman, D. J.; Teuscher, J.; Pathak, S.; Avolio, R.; D'Errico, G.; Vitiello, G.; Fantacci, S.; Snaith, H. J. *J. Am. Chem. Soc.* **2013**, *135* (36), 13538.

Table of Contents artwork